Vehicle-to-vehicle Angular Determinations by Means of DSRC Signals

Ilya V. Korogodin, Evgeniy N. Boldenkov and Vladimir V. Dneprov
Moscow Power Engineering Institute, Russia

BIOGRAPHY

Ilya V. Korogodin is an Associated Professor at the Radio Engineering Systems Department at the Moscow Power Engineering Institute since September 2013. He received his Ph.D. (candidate of sciences) degree in Radar and Radio-Navigation technologies in 2013. His research interests include digital GNSS signal processing, GLONASS evaluation, constellation simulation, multiantenna systems and ASICs.

Evgeniy N. Boldenkov was an Associated Professor at the Radio Engineering Systems Department at the Moscow Power Engineering Institute. He received his Ph.D. degree in 2007.

Vladimir V. Dneprov is a postgraduate at the Radio Engineering Systems Department at the Moscow Power Engineering Institute. He obtained his Master degree in radio systems in 2014. His research interests are GNSS signal processing and attitude determination.

ABSTRACT

In this paper we describe a relative vehicle-to-vehicle (V2V) attitude estimation approach, an algorithm, experimental results and analysis of error sources. An innovative step of the presented approach is a utilization of DSRC signals for relative angular measurements between vehicles. Positioning methods based on ranging measurements suffer from the problem of poor geometric factor. The relative angular measurements can make a significant contribution to the positioning accuracy and reliability. It is proposed to install a DSRC transceiver with several antennas on each vehicle. Each antenna radiates a unique signal and receives signals from other vehicles. It allows measuring attitude of the vehicles relatively to their line of sight. The attitude is described by angle-of-arrival (AoA) and angle-of-departure (AoD). An estimation algorithm for the angles is designed. The algorithm utilizes a phases-to-direction interrelation model; the model was calculated for a proposed antenna system by means of an electromagnetic simulation. This simulation shows that the mutual influence of the antennas can disturb angle estimations about 10 degrees. The proposed algorithm allows considering the certain radiation patterns and mitigating the influence effects, that is confirmed by the experiment. Commercial-off-the-shelf Wi-Fi modules were used for the experiments. Wi-Fi 802.11n and DSRC 802.11p signals have close carrier frequencies, power and packet structures. It allows extrapolating the experimental results to DSRC. A front-end delay calibration methodology is presented. In accordance with the methodology the receiver is slowly and uniformly rotated and amendments to the phases are calculated. The experiments were conducted under good (open field) and bad (multistory parking) signal propagation conditions. The AoA/AoD accuracy about 5-15 degrees (peak) is shown. The multipath errors don't dominate in the direct line-of-sight conditions. Multipath propagation causes errors up to 10 degrees (peak). The mutual influence of antenna elements and car body causes errors up to 10 degrees (peak).

INTRODUCTION

Mutual V2V angular measurements are useful in many applications: unmanned driving, driver assistance, cooperative positioning, etc. For example, the relative angular measurements can make a significant contribution to the accuracy and reliability of relative positioning of vehicles. Positioning methods based only on ranging measurements suffer from the problem of poor geometric factor. In most driving situations a chain of cars is stretched in one direction along a road. As a result, it is possible to achieve good resolution along the road, but it is very difficult to estimate your position across the road. This problem can be solved by utilizing angular measurements [Cheong2015]. In conjunction with ranges, angles allow you to determine your position and orientation relative to the other vehicles accurately.

The angular system calculates mutual direction to another cars (an angle between the line-of-sight and car axis, for instance). It can be implemented by processing of signals transmitted from another car (see Figure 1). Moreover, it is possible to measure the second angle between the transmitting car and the line-of-sight by the principle of reciprocity. For this purpose the transmitter must radiate either several signals or a signal with space dependence of power.

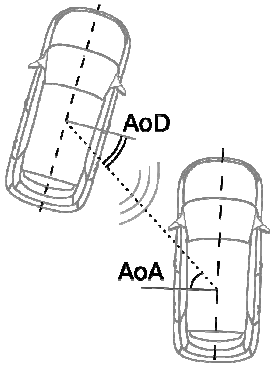

Figure 1 – Vehicle-to-vehicle angular determinations

When the cars have exchanged the transmitter/receiver roles, each of the cars has independent measurements of these angles. So, they can compare their results and control the results quality.

In this study we consider DSRC IEEE 802.11p as such measurement signals. DSRC is a widespread system, very similar to the civil WiFi. There are OFDM signals with about 5.8-5.9 GHz carrier frequencies. The DSRC signals have wide bandwidth (from 10 to 20 MHz) and are strong enough (from 15 to 35-45 dBm of emitted power) [SAEJ2945/1, SAEJ2735, ETSIES202663, IEEE802.11p]. In contrast to WiFi the system packets has low latency. There are short safety messages with time multiplexing between vehicles [IEEE1609.4] in modern standards, based on DSRC. The safety messages are Basic Safety Message (BSM) in the USA standards [SAEJ2945/1, SAEJ2735] and Cooperative Awareness Message (CAM) in the Europe standards [ETSITS102 637-2]. BSM has a period of 100 ms and a total length about 300 bytes, CAM has a default period of 500 ms and a total length about 800 bytes.

While ranging technique is tricky to implement in a framework of current IEEE 802.11p, angles measurement approach doesn't have such limitations. In the following sections an angles estimation algorithm, simulation and experimental results and analysis of error sources are discussed.

SIGNAL PROCESSING ALGORITHM

Let's consider observations of complex OFDM signals by *M* receiving antennas (see Figure 2). Each signal contains *K* subcarriers and is transmitted from own antenna. Let *N* be a total amount of the transmitting antennas (and signals).

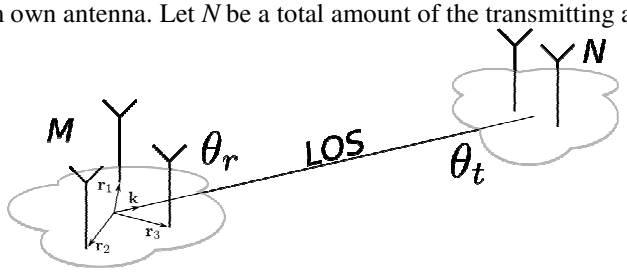

Figure 2 – Line-of-sight between the receiver and the transmitter

The observations are obtained in a time interval; we repeated them *L* times during the interval. Let *n* be an index of a transmitting antenna, *m* be an index of a receiving antenna, *k* be a subcarrier index, *l* be a time (packet) index in whole this report. The observations mathematic model is:

$$\mathbf{y}_l = \sum_{k=1}^{K}\sum_{n=1}^{N}\mathbf{S}_{k,n,l} + \mathbf{n}_l, \tag{1}$$

where $\mathbf{y}_l = \left| y_{1,l} \quad \ldots \quad y_{M,l} \right|^T$ is the observations (ADC signals, for example) vector for the l-th point of time, $\mathbf{n}_l$ is a complex AWGN with the $\mathbf{N}$ covariance matrix.

The antenna systems are described by their steering vectors. Steering vector can be treated as a vector of antenna system output complex signals (normalized to any of them) while the system is receiving a test signal from the $\boldsymbol{\theta}$ direction. The direction may be expressed as angles, quaternion, etc.

Let $\mathbf{H}_{t,k} = \mathbf{H}_{t,k}\left(\boldsymbol{\theta}_t\right)$ be a transmitter steering amplitude-phase vector $\left(N \times 1\right)$ for a $\boldsymbol{\theta}_t$ direction and the *k*-th subcarrier, $\mathbf{H}_{r,k} = \mathbf{H}_{r,k}\left(\boldsymbol{\theta}_r\right)$ be a receiver steering vector $\left(M \times 1\right)$ for a $\boldsymbol{\theta}_r$ direction, then the signal vector $\mathbf{S}_{k,n,l}$ can be written as:

$$\mathbf{S}_{k,n,l} = \mathbf{S}_{k,n,l}\left(\boldsymbol{\theta}_r, \boldsymbol{\theta}_t\right) = \mathbf{H}_{k,n}\left(\boldsymbol{\theta}_r, \boldsymbol{\theta}_t\right) G_{k,n,l} e^{j\varphi_k}, \tag{2}$$

where φ_k is a random initial phase for the *k*-th subcarrier ($\boldsymbol{\varphi} = \left|\varphi_1 \quad .. \quad \varphi_K\right|^T$), $\mathbf{H}_{k,n}$ is the *n*-th column of $\mathbf{H}_{r,k}\mathbf{H}_{t,k}^T$ matrix, $G_{k,n,l}$ is the *k*-th subcarrier signal of the n-th transmitter antenna (ω_0 and ω_k is an intermediate and the *k*-th subcarrier frequency, t_l is the *l*-th time moment):

$$G_{k,n,l} = h_{k,n,l} \exp\left(j\left(\omega_0 + \omega_k\right) t_l \right). \tag{3}$$

We will consider the modulation function $h_{k,n,l}$ as known. It can be obtained due to a data demodulation procedure before the angle measurements processing.

The model (1) contains three unknown random vectors: the LOS direction $\boldsymbol{\theta}_t$ for the transmitter, the LOS direction $\boldsymbol{\theta}_r$ for the receiver and the initial phases $\boldsymbol{\varphi}$. Let's estimate the parameters. We will minimize the mean risk for the simple loss function, so we should find the maximum of the posteriori probability density [Tihonov1991]:

$$\left\{\hat{\boldsymbol{\theta}}_t, \hat{\boldsymbol{\theta}}_r, \hat{\boldsymbol{\varphi}}\right\} = \underset{\boldsymbol{\theta}_t, \boldsymbol{\theta}_r, \boldsymbol{\psi}}{\arg\max} \left\{ p\left(\boldsymbol{\theta}_t, \boldsymbol{\theta}_r, \boldsymbol{\varphi} \middle| \mathbf{y}_1^T\right) \right\}, \tag{4}$$

where the posteriori probability density (p_{pr} is a priori probability, *c* is a constant):

$$p\left(\boldsymbol{\theta}_t, \boldsymbol{\theta}_r, \boldsymbol{\varphi} \middle| \mathbf{y}_1^L\right) = c p_{pr}\left(\boldsymbol{\theta}_t, \boldsymbol{\theta}_r\right) p\left(\mathbf{y}_1^L \middle| \boldsymbol{\theta}_t, \boldsymbol{\theta}_r, \boldsymbol{\varphi}\right). \tag{5}$$

Here we consider the $\boldsymbol{\varphi}$ components priori density as uniform at $[0; 2\pi]$, the parameters are independent to each over. The assumption is rough enough, but it allows to synthesize the more sustainable to propagation conditions algorithm.

If the priori distributions of $\boldsymbol{\theta}_t$ and $\boldsymbol{\theta}_r$ are Gaussian with covariance matrixes $\mathbf{D}_{pr,t}$ and $\mathbf{D}_{pr,r}$, mean values $\boldsymbol{\theta}_{pr,t}$ and $\boldsymbol{\theta}_{pr,r}$, then equation (4) transforms to:

$$\left\{\hat{\boldsymbol{\theta}}_t, \hat{\boldsymbol{\theta}}_r, \hat{\boldsymbol{\varphi}}\right\} = \underset{\boldsymbol{\theta}_t, \boldsymbol{\theta}_r, \boldsymbol{\psi}}{\arg\max} \left\{ -\frac{1}{2}\left\|\boldsymbol{\theta}_t - \hat{\boldsymbol{\theta}}_{pr,t}\right\|_{D_{pr,t}}^2 - \frac{1}{2}\left\|\boldsymbol{\theta}_r - \hat{\boldsymbol{\theta}}_{pr,r}\right\|_{D_{pr,r}}^2 - \frac{1}{2}\sum_{l=1}^{L}\left\|\mathbf{y}_l - \sum_{k=1}^{K}\sum_{n=1}^{N}\mathbf{S}_{k,n,l}\left(\boldsymbol{\theta}_t, \boldsymbol{\theta}_r, \boldsymbol{\varphi}\right)\right\|_{\mathbf{N}}^2 \right\}, \tag{6}$$

where $\|\mathbf{v}\|_{\mathbf{N}}^2 = \mathbf{v}^+\mathbf{N}^{-1}\mathbf{v}$ is a quadratic form, $\mathbf{v}^+$ is the Hermitian transpose.

The third term can be transformed to the form:

$$\sum_{l=1}^{L}\left\|\mathbf{y}_l - \sum_{k=1}^{K}\sum_{n=1}^{N}\mathbf{S}_{k,n,l}\left(\boldsymbol{\theta}_t, \boldsymbol{\theta}_r, \boldsymbol{\varphi}\right)\right\|_{\mathbf{N}}^2 = \sum_{l=1}^{L}\left\|\mathbf{y}_l\right\|_{\mathbf{N}}^2 - \sum_{k=1}^{K}\sum_{n=1}^{N}\left\|\mathbf{q}_{n,k}\right\|_{\mathbf{N}}^2 + \sum_{k=1}^{K}\sum_{n=1}^{N}\left\|\mathbf{q}_{n,k} - \mathbf{H}_{k,n}\left(\boldsymbol{\theta}_r, \boldsymbol{\theta}_t\right)e^{j\varphi_k}\right\|_{\mathbf{N}}^2, \tag{7}$$

where

$$\mathbf{q}_{k,n} = \sum_{l=1}^{L}\mathbf{y}_l G_{n,k,l}^+ \tag{8}$$

are the correlation sums vector for the k-th subcarrier of the n-th transmitted signal.

Let's estimate the $\boldsymbol{\varphi}$ components. For fixed $\boldsymbol{\theta}_t, \boldsymbol{\theta}_r$ the maximum of (6) corresponds to

$$\hat{\varphi}_k\left(\boldsymbol{\theta}_t, \boldsymbol{\theta}_r\right) = \underset{\boldsymbol{\varphi}}{\arg\min}\left\{\sum_{n=1}^{N}\left\|\mathbf{q}_{k,n} - \mathbf{H}_{k,n}\left(\boldsymbol{\theta}_r, \boldsymbol{\theta}_t\right)e^{j\varphi_k}\right\|_{\mathbf{N}}^2\right\} \tag{9}$$

The quadratic form is (for the case of diagonal matrix $\mathbf{N}$ with elements σ^2)

$$\sum_{n=1}^{N}\left\|\mathbf{q}_{n,k} - \mathbf{H}_{k,n}\left(\boldsymbol{\theta}_r, \boldsymbol{\theta}_t\right)e^{j\varphi_k}\right\|_{\mathbf{N}}^2 = \sum_{n=1}^{N}\left\|\mathbf{q}_{k,n}\right\|_{\mathbf{N}}^2 - 2\,\mathrm{Re}\left\{\frac{1}{\sigma^2}\mathbf{H}_{k,n}^+\left(\boldsymbol{\theta}_t, \boldsymbol{\theta}_r\right)\mathbf{q}_{k,n}e^{-j\varphi_k}\right\} + \frac{1}{\sigma^2}\mathbf{H}_{k,n}^+\left(\boldsymbol{\theta}_t, \boldsymbol{\theta}_r\right)\mathbf{H}_{k,n}\left(\boldsymbol{\theta}_t, \boldsymbol{\theta}_r\right), \tag{10}$$

where only the second term depends on initial phase, so

$$\hat{\varphi}_k\left(\boldsymbol{\theta}_t, \boldsymbol{\theta}_r\right) = \underset{\boldsymbol{\varphi}}{\arg\max}\left\{\mathrm{Re}\left\{e^{-j\varphi_k}\sum_{n=1}^{N}\frac{1}{\sigma^2}\mathbf{H}_{k,n}^+\left(\boldsymbol{\theta}_t, \boldsymbol{\theta}_r\right)\mathbf{q}_{k,n}\right\}\right\}. \tag{11}$$

The desired maximum is achieved when $\mathrm{Re}\left\{e^{-j\varphi_k}\sum_{n=1}^{N}\frac{1}{\sigma^2}\mathbf{H}_{k,n}^+\left(\boldsymbol{\theta}_t, \boldsymbol{\theta}_r\right)\mathbf{q}_{k,n}\right\} = \left|\sum_{n=1}^{N}\frac{1}{\sigma^2}\mathbf{H}_{k,n}^+\left(\boldsymbol{\theta}_t, \boldsymbol{\theta}_r\right)\mathbf{q}_{k,n}\right|$, where $|x|$ is the absolute value of the complex number x. In this case:

$$\hat{\varphi}_k = \arg\sum_{n=1}^{N}\frac{1}{\sigma^2}\mathbf{H}_{k,n}^+\left(\boldsymbol{\theta}_t, \boldsymbol{\theta}_r\right)\mathbf{q}_{k,n}. \tag{12}$$

The equations (7), (10), (12) in (6) give

$$\left\{\hat{\boldsymbol{\theta}}_t,\hat{\boldsymbol{\theta}}_r\right\}=\arg\max_{\boldsymbol{\theta}_t,\boldsymbol{\theta}_r}\left\{-\frac{1}{2}\left\|\boldsymbol{\theta}_t-\hat{\boldsymbol{\theta}}_{pr,t}\right\|^2_{D_{pr,t}}-\frac{1}{2}\left\|\boldsymbol{\theta}_r-\hat{\boldsymbol{\theta}}_{pr,r}\right\|^2_{D_{pr,r}}+\right.$$
$$\left.+\frac{1}{\sigma^2}\sum_{k=1}^{K}\left|\sum_{n=1}^{N}\mathbf{H}^{+}_{k,n}\left(\boldsymbol{\theta}_t,\boldsymbol{\theta}_r\right)\mathbf{q}_{k,n}\right|-\sum_{k=1}^{k}\sum_{n=1}^{N}\frac{1}{\sigma^2}\mathbf{H}^{+}_{k,n}\left(\boldsymbol{\theta}_t,\boldsymbol{\theta}_r\right)\mathbf{H}_{k,n}\left(\boldsymbol{\theta}_t,\boldsymbol{\theta}_r\right)\right\}. \tag{13}$$

If we have no priori information and power radiation pattern of the antennas doesn't depend on direction (constant signal-to-noise ratio), then we can simplify the directions estimation algorithm:

$$\left\{\hat{\boldsymbol{\theta}}_t,\hat{\boldsymbol{\theta}}_r\right\}=\arg\max_{\boldsymbol{\theta}_t,\boldsymbol{\theta}_r}\left\{\sum_{k=1}^{K}\left|\sum_{n=1}^{N}\mathbf{H}^{+}_{k,n}\left(\boldsymbol{\theta}_t,\boldsymbol{\theta}_r\right)\mathbf{q}_{k,n}\right|-\sum_{k=1}^{k}\sum_{n=1}^{N}\frac{1}{\sigma^2}\mathbf{H}^{+}_{k,n}\left(\boldsymbol{\theta}_t,\boldsymbol{\theta}_r\right)\mathbf{H}_{k,n}\left(\boldsymbol{\theta}_t,\boldsymbol{\theta}_r\right)\right\}. \tag{14}$$

If radiation pattern of each antenna doesn't depend on direction (the signal-noise-ratio doesn't depend on direction), then the algorithm transforms to:

$$\left\{\hat{\boldsymbol{\theta}}_t,\hat{\boldsymbol{\theta}}_r\right\}=\arg\max_{\boldsymbol{\theta}_t,\boldsymbol{\theta}_r}\left\{\sum_{k=1}^{K}\left|\sum_{n=1}^{N}\mathbf{H}^{+}_{k,n}\left(\boldsymbol{\theta}_t,\boldsymbol{\theta}_r\right)\mathbf{q}_{k,n}\right|\right\}. \tag{15}$$

The algorithm prescribes several steps (see Figure 3):

1. Receive and store the signals.
2. Demodulate the signals; check the data (possible including $\mathbf{H}_{t,k}\left(\boldsymbol{\theta}_t\right)$ function).
3. Restore signal form $G_{k,n,l}$ from the data.
4. Calculate the correlation sums $\mathbf{q}_{k,n}$ for each subcarrier and each transmitter dataflow.
5. Load priori steering vector functions $\mathbf{H}_{t,k}\left(\boldsymbol{\theta}_t\right)$ and $\mathbf{H}_{r,k}\left(\boldsymbol{\theta}_r\right)$ for the transmitter and receiver antenna systems.
6. Iterate over $\boldsymbol{\theta}_t$ and $\boldsymbol{\theta}_r$, find maximum for (13) (if you have a priori information) or (14) (if you have no priori information). The required estimates are the relevant arguments $\hat{\boldsymbol{\theta}}_t$, $\hat{\boldsymbol{\theta}}_r$ of the maximum.

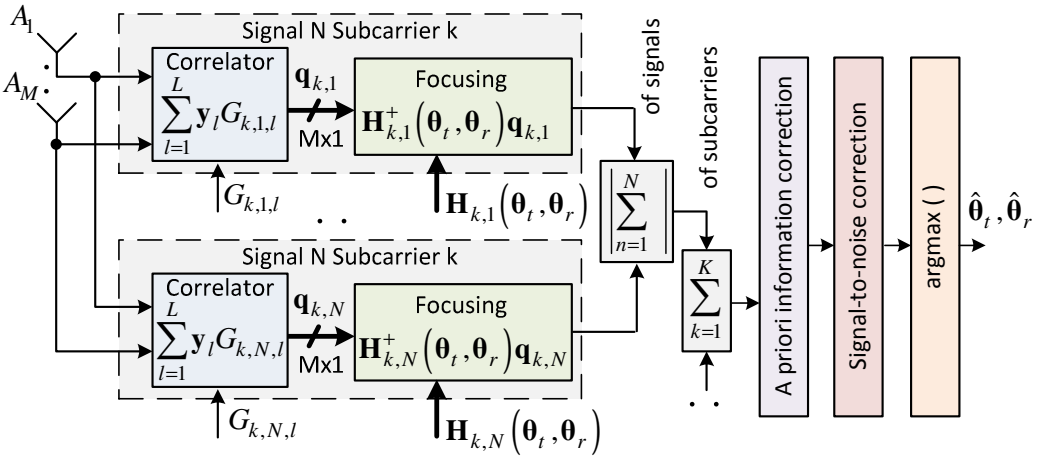

Figure 3 – The angle of arrival/departure estimation algorithm

Let's consider a simple case of independent omnidirectional antennas in the antenna system. Let $\mathbf{r}_m$ be a coordinate vector of the *m*-th antenna in a XYZ frame (see Figure 2). Let $\mathbf{k}$ be a unit vector of the receiver-transmitter LOS in the frame. In this case the phase differences are described by scalar products $\mathbf{k}^T\mathbf{r}_m$, all amplitudes are equal and the steering vector is:

$$\mathbf{H}_k\left(\boldsymbol{\theta}_r\right)=\left|\exp\left(j\frac{\left(\omega_0+\omega_k\right)}{c}\mathbf{k}^T\left(\boldsymbol{\theta}\right)\left(\mathbf{r}_1-\mathbf{r}_1\right)\right)\ \ ..\ \ \exp\left(j\frac{\left(\omega_0+\omega_k\right)}{c}\mathbf{k}^T\left(\boldsymbol{\theta}\right)\left(\mathbf{r}_M-\mathbf{r}_1\right)\right)\right|^T, \tag{16}$$

where *c* is the speed of light.

We can express the steering vector (16) elements for the *k*-th subcarrier through the vector elements for the intermediate frequency:

$$H_{k,m}\left(\boldsymbol{\theta}\right)=\exp\left(j\frac{\omega_0}{c}\mathbf{k}^T\left(\boldsymbol{\theta}\right)\left(\mathbf{r}_m-\mathbf{r}_1\right)\right)\cdot\exp\left(j\frac{\omega_k}{c}\mathbf{k}^T\left(\boldsymbol{\theta}\right)\left(\mathbf{r}_m-\mathbf{r}_1\right)\right). \tag{17}$$

It is possible to use (17) as a good assumption for any configuration of the antenna system, but it still requires the antenna coordinates:

$$H_{k,m}(\boldsymbol{\theta}) \approx H_{0,m}(\boldsymbol{\theta}) \cdot \exp\left(j\frac{\omega_k}{c}\mathbf{k}^T(\boldsymbol{\theta})\left(\mathbf{r}_m - \mathbf{r}_1\right)\right), \tag{18}$$

where $H_{0,m}(\boldsymbol{\theta})$ is the steering vector of the antenna system at the intermediate frequency. It can be obtained through an electromagnetic simulation or an anechoic chamber experiment as the radiation patterns ratio for antenna ports.

ANTENNA SYSTEM

There is a plenty of possible antenna configurations, it is a multicriterial task to choose an antenna system. The equation (13) is suitable for amplitude direction finders, interferometers and any their mixes. In this study we chose uniform linear array of omnidirectional antennas for our simulations and experiments. The proposed design of the antenna system is depictured on the Figure 4. Three vibrators are located on the metal plate. The distance between them is about a half of the wave length (50/2=25 mm). The length is about a quarter of the wave length (50/4=12 mm). The radio-transparent cap covers the vibrators.

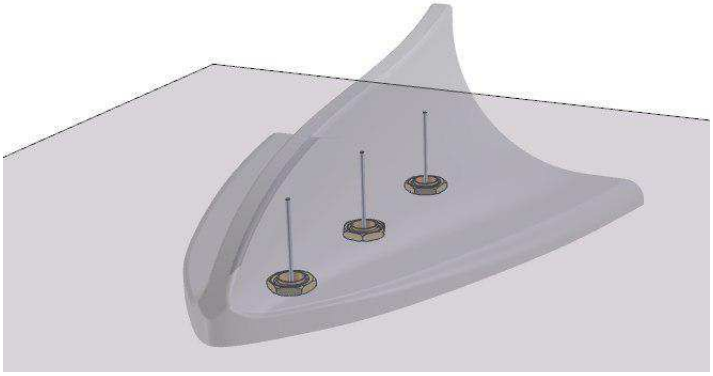

Figure 4 – DSRC antenna system design

There are several reasons of the choice. It is possible to transfer data by means of DSRC in the no-line-of-sight conditions. But we need the direct visibility for the angles estimations. We should place the antennas on the car body to achieve the line-of-sight. The number of antennas allows to control measurements and interpret them easy. The length between vibrators allows to resolve a phase ambiguity. The vibrators length allows to reconcile the impedance and to minimize the antenna's height.

Let's consider the phase difference for signals in the horizontal plane for the antennas as a function of the angle-of-arrival (θ on the Figure 8). For a uniform linear array of independent antennas this function is the sinus (from (16)):

$$\psi_{indep,m1,k}(\theta) = \frac{(\omega_0 + \omega_k)}{c}\mathbf{k}^T\left(\mathbf{r}_m - \mathbf{r}_1\right) = \frac{(\omega_0 + \omega_k)l_{m1}}{c}\sin(\theta), \tag{19}$$

where l_{m1} is the distance between the *m*-th and the first antennas. In this case the steering vector can be written as:

$$\mathbf{H}_{indep,k}(\theta) = \left|1 \quad \exp\left(j\psi_{indep,21,k}(\theta)\right) \quad .. \quad \exp\left(j\psi_{indep,M1,k}(\theta)\right)\right|^T . \tag{20}$$

ERRORS CAUSED BY THERMAL NOISE

A computer simulation was performed for the synthesized algorithm and the chosen antenna system. An overtaking maneuver was simulated. The designed model includes transceivers on two vehicles, a direct line-of-sight propagation model and the synthesized estimation algorithm. DSRC signal is emitted by the three vibrators described above. Each antenna broadcasts own subcarrier set as it is shown on the Figure 5.

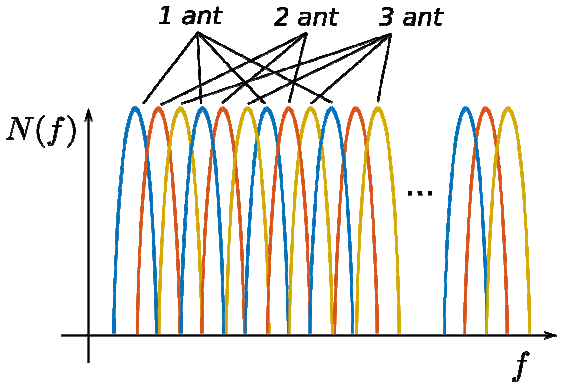

Figure 5 – Subcarriers distribution for transmitting antennas

The payload length is 300 bytes [IEEE1609.3, SAEJ2735]. Common transmitting power is 15 dBm. Power spectrum density of the receiver noise is -170 dBm/Hz.

The simulation shows that the synthesized algorithm works correctly. Estimation errors, caused by the receiver noise, are low.

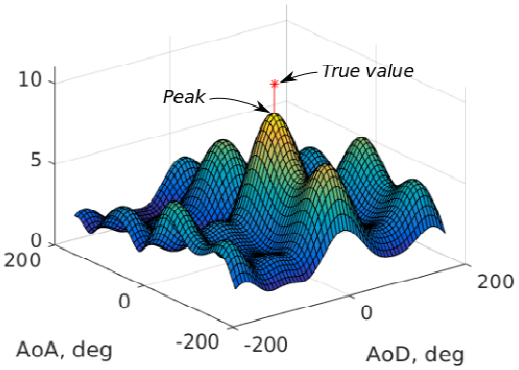

Figure 6 – Posterior surface

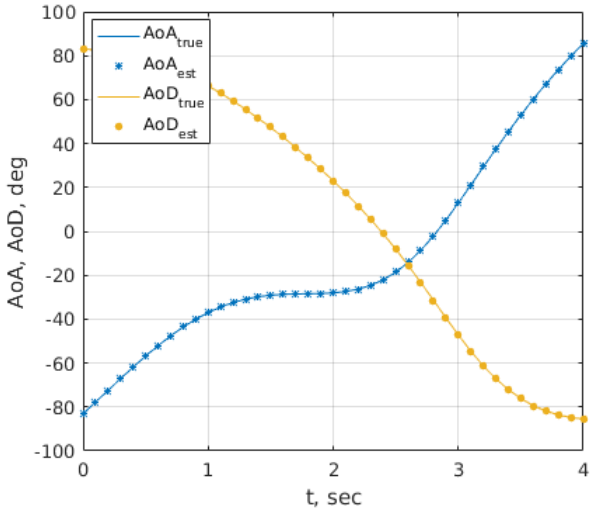

Figure 7 – Estimated and true angles during the overtaking maneuver

By analogy with Wi-Fi [Wong2008, Tsur2015, Schüssel 2016] and GNSS, it can be assumed that these thermal errors are negligible in comparison with the multipath errors, the mutual influence of the antennas, calibration, etc.

ELECTROMAGNETIC SIMULATION

Unlike GNSS goniometers, the presented antennas are located close enough. It is too rough to consider them as independent ones. They influence on each other. The dependence of the phase difference from angle of arrival is complex; it is different from the similar function for the independent antennas. It is possible to estimate this difference $\varepsilon_\psi = \psi - \psi_{indep}$ by means of a simulation.

An electromagnetic model of the antenna system was developed into CST Microwave Studio (see Figure 8). The model is close to the experimental setup, which will be described in the relevant section. There is a ground plane, three $\lambda/4$ vibrators and coaxial cables in the model. The ground plane is a 15x15 cm perfect electric conductor plate. The antennas are continued cores of relevant cables. Their diameter is 1.1 mm. The distance between close pairs is $\lambda/2$. The diameter of dielectric parts of the cables is 3.92 mm. Braids of the cables have 6 mm diameter and are connected to the ground plane. There are three ports at a distance of 1 cm from the plate.

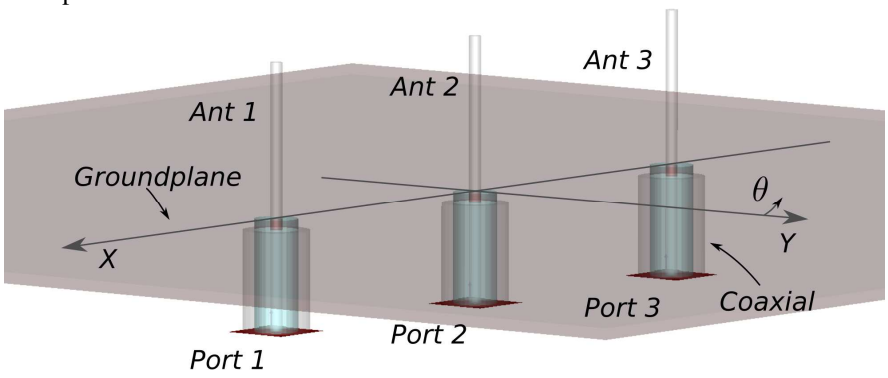

Figure 8 – CST Microwave Studio antenna model

Simulation results contain power and phase radiation patterns for each port. Due to the symmetry of the model results for the first and the third antennas (ports) are the same, so we should discuss differences between the middle and any side antenna. Similarly, it suffices to consider phase differences ψ_{31} and ψ_{21} for the third and for the second antennas with respect to the first one.

Power radiation patterns in the horizontal plane for the vertical polarization are presented on the Figure 9. The patterns both are not circular and are not equal. The difference between them reaches about 2 dB. An irregularity of the side antenna radiation pattern is about 5 dB.

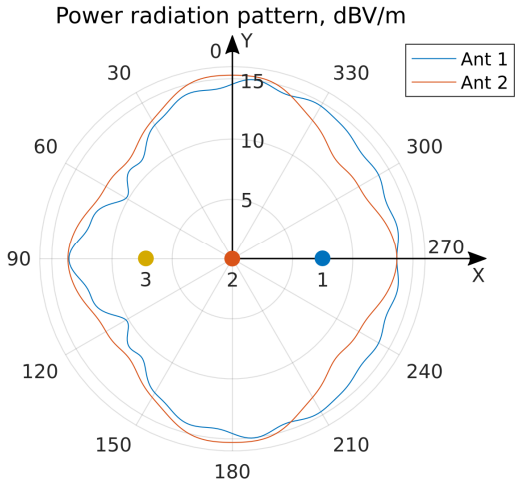

Figure 9 – Power radiation patterns in the horizontal plane for the vertical polarization

Although the amplitude depends on the direction, this dependence is weak in comparison with same dependence for phases. Phase radiation patterns are presented on the Figure 10. The patterns are significantly different in the horizontal plane. The difference allows estimating AoA/AoD by means of the phase comparison. The fact is the basis of all interferometry approaches.

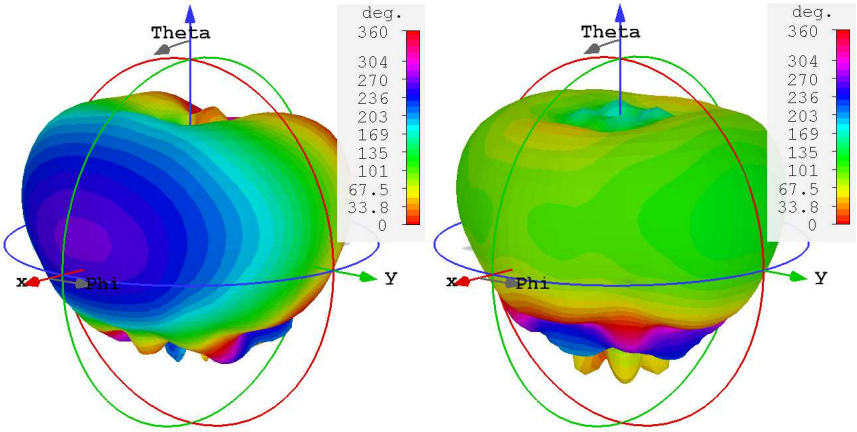

a) b)

Figure 10 – Phase radiation patterns for the theta-component of the field: a) antenna 1; b) antenna 2

Let's compare the phase differences profiles obtained through simulation and calculated by means of the equation (19) for the case of the independent antennas. The phase differences as the function of the angle in the horizontal plane are presented on the Figure 11.

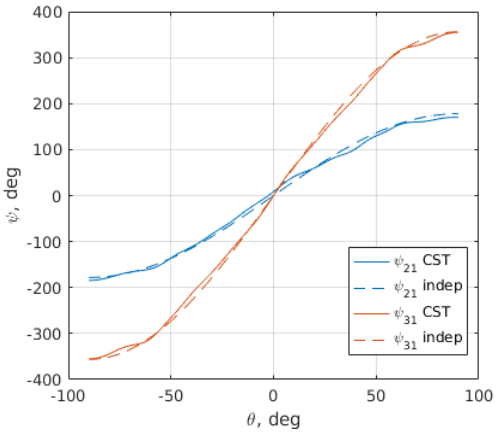

Figure 11 – Phase differences for the CST model and for the independent antennas model

The CST phase differences functions are close to the same results for the independent antennas, but there is a little divergence, up to 10-20 degrees (see Figure 12).

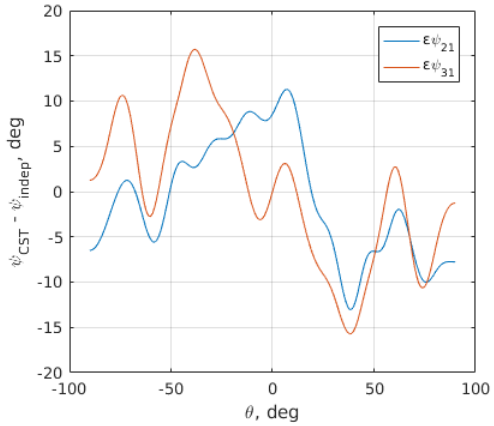

Figure 12 – Divergence between phase differences for CST and independent antennas models

As conclusion, if we don't take into account the amendment, then the divergence can cause the AoA/AoD estimation error up to 10 degrees (see Figure 13).

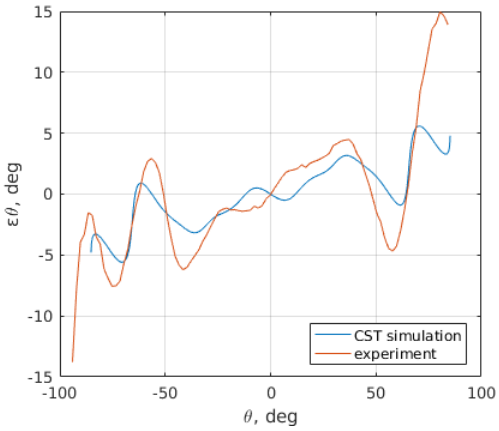

Figure 13 – Angle estimation error caused by the antennas mutual influence

EXPERIMENTAL RESULTS

As shown above, the thermal noise is not the main source of angle estimation errors in real propagation conditions. It can be assumed, and tests proofed the assumption, that a multipath, an inaccurate calibration, radiation pattern disturbances cause larger errors. But it is too difficult to estimate those factors by means of mathematical models only.

The curtain multipath errors depend on amplitude, phase and direction of a reflected signal. There are several studies [Yin 2006, Acosta-Marum2007, Islam2013, Cheong2015, Kukolev2015] of propagation channel characteristics for different conditions. Also the 802.11-14/0259r0 document, an amendment to the 802.11 standard, specifies 802.11 V2V radio channel models for fading conditions that can be used during simulation [Keysight2016]. The documents are focused on big delay intervals and channel models, which are worth for intersymbol interference researches, but are insufficient to assess the impact on the angular measurements.

The effect of mutual antenna influences to the radiation pattern disturbance was estimated by electromagnetic simulation above. But it is the first step only, there are a plenty of impacting factors in the real world.

Mockups

Several experiments to evaluate the effect of these phenomena on the angular measurements were conducted. We implemented our mockup using off-the-shelf Intel 5300 WiFi 802.11n cards. Wi-Fi 802.11n and DSRC 802.11p signals have a close carrier frequency (5.3 GHz vs 5.9 GHz), power and a packet structure and duration (WiFi symbol two times shorter). The difference of signal bandwidth was compensated by utilizing only a part of subcarriers in the signal processing algorithm. It allows extrapolating the experimental results to DSRC.

We employed Linux CSI tool [Halperin, 2011] to obtain the amplitudes and phases of subcarriers. The measurements are quantized, i.e., each of real and imaginary parts is represented using 8 bits. The WiFi cards operate in 5 GHz WiFi spectrum, the speed rate is 6 Mb/s. Both the transmitter and the receiver operate in injection mode. The modules are mounted into Lenovo Q180 PCs, controlled by Kubuntu 14.04.

Both the transmitter and the receiver has got hand-made antenna system (see Figure 14). The system is corresponding to the one described above (see Figure 4).

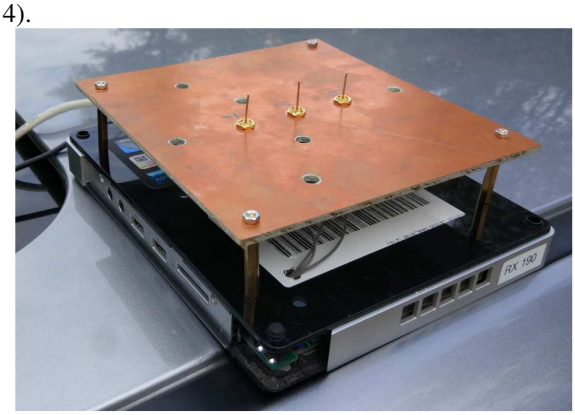
Figure 14 – The receiver mockup on the car roof

Calibration procedure

The mockup measurements are shifted by delays in the branches of the receiver front-end. The delays (caused shifts in phase differences) must be compensated by any calibration procedure. The several calibration approaches are known [Korogodin12, Tsur15]. But we didn't manage to achieve stable results by the approaches in our configuration.

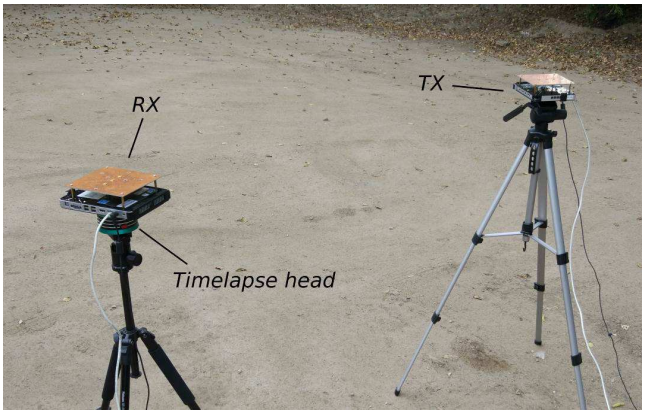

Figure 15 – The calibration procedure in process

The goal of the calibration procedure is to get two values of phase corrections: for the second and for the third antenna. To achieve this result we placed the mockups on tripods in the open space, moreover we used a timelapse slow rotating head for the receiver tripod (see Figure 15). The REVO EPH-6 was used for this purpose. The head allows to rotate the receiver evenly and very slowly (180 degrees per 15 minutes).

We start the measurement collection when the receiver and the transmitter antennas are aligned in the line (see Figure 16). The fact of alignment can be checked by a laser beam. The master laptop initiates measurements evenly with 3 seconds step. Every 3 seconds the transmitter broadcasts 50 packets with 512 bit payload and the receiver gets and stores them. The data acquisition must be stopped when the receiver has done a half-turn and the antennas are aligned again.

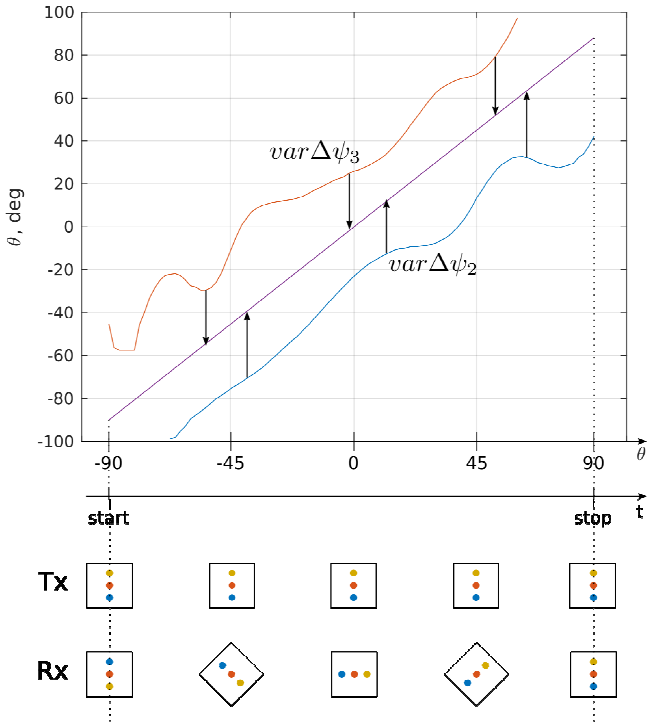

Figure 16 – Angle during calibration procedure: estimations by means of the first and the second antennas (blue), estimations by means of the second and the third antennas (red), true angle value (purple)

As result, we get measurements signed by the true angle value: the first observation corresponds to -90 degrees, the last one corresponds to +90 degrees, the middle observations are uniformly distributed from -90 to +90 degrees.

After several experiments in different distances between TX and RX we find the desired calibration shifts. For this purpose the angle estimations are calculated by means of described above algorithm. We use observations from two antennas only: separately 2 and 1, separately 3 and 2. The desired shifts are calculated by means of minimizing of the sum residual for the angle estimations:

$$\Delta\psi_2, \Delta\psi_3 = \arg\min\left(\sum_{\exp}\sum_{l=1}^{L}\left(\hat{\theta}_{21,l} - \theta_l\right)^2 + \left(\hat{\theta}_{32,l} - \theta_l\right)^2\right) \tag{21}$$

The calibration was performed both for the receiver and for the transmitter.

Mutual antennas influence

After the calibration the mockups can be used for the angles estimation procedure.

As the first step, we checked the CST simulation results. We processed the open space observations (obtained during the calibration procedure) using the independent antennas model (19). The CST simulation predicts significant angle estimations error in this case. Our experimental results proof this assertion (see Figure 13). The obtained error function is close enough to the simulated one. As conclusion, we must consider the antennas mutual influence to achieve high accuracy. Otherwise, the error would be about ten degrees.

Angles estimation errors in good condition

We performed several experiments with both the receiver and the transmitter mounted on the tripods under the good propagation conditions. The tripods were located far from buildings and cars (tens of meters). In these experiments either the receiver or the transmitter was rotated. The experiments methodology was similar to described in the calibration subsection.

The quality of the conditions is good presented by the channel flatness and phase differences histograms. Under good conditions the histograms are sharp (see Figure 17, a).

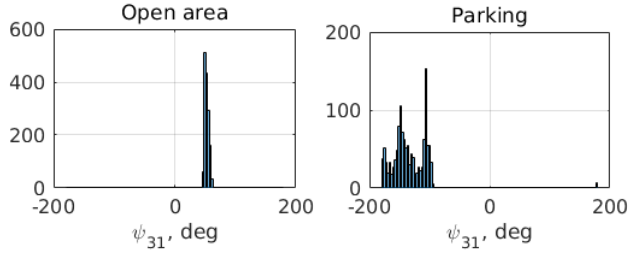

a) b)

Figure 17 – Phase difference histogram examples: a) open area; b) parking

The obtained observations were processed using the CST antenna model. We got errors about 5 degrees peak value in the open space conditions. The graph of AoA estimation error is presented on the Figure 18 (the blue curve).

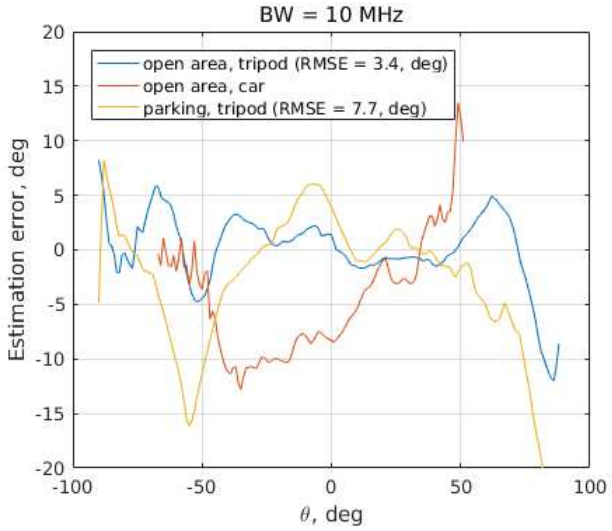

Figure 18 – AoA estimation errors (CST RPs are used)

We have got similar accuracy for AoD, but the processing of the observation in the case of rotating transmitter is complex because of the Intel 5300 board features. The board heterodynes reinitialize sometimes. It causes the 90 degree ambiguity in the phase differences calculated for different transmitter antennas. We resolved the ambiguity by hands, but it is very time wasting procedure. So, next studies are focused on the AoA.

Car body influence

The experiment with a car was performed to consider the car body influence to the angle estimations. We need the true angle values to calculate estimation error. It is hard to rotate the car evenly, so we modified the methodology to get the values.

Figure 19 – The car experiment in process (open area)

The receiver is located on the car roof. The vehicle is connected with a column by means of a cable via an electric winch (see Figure 19). The electric winch moves the car evenly and slowly (30 cm/min) from the start to the finish point. As result, the true position of the car is known for any time. The transmitter is located aside from the car trajectory (1.9 m). The true angle value can be calculated for each car position and be compared with obtained measurements (see Figure 20).

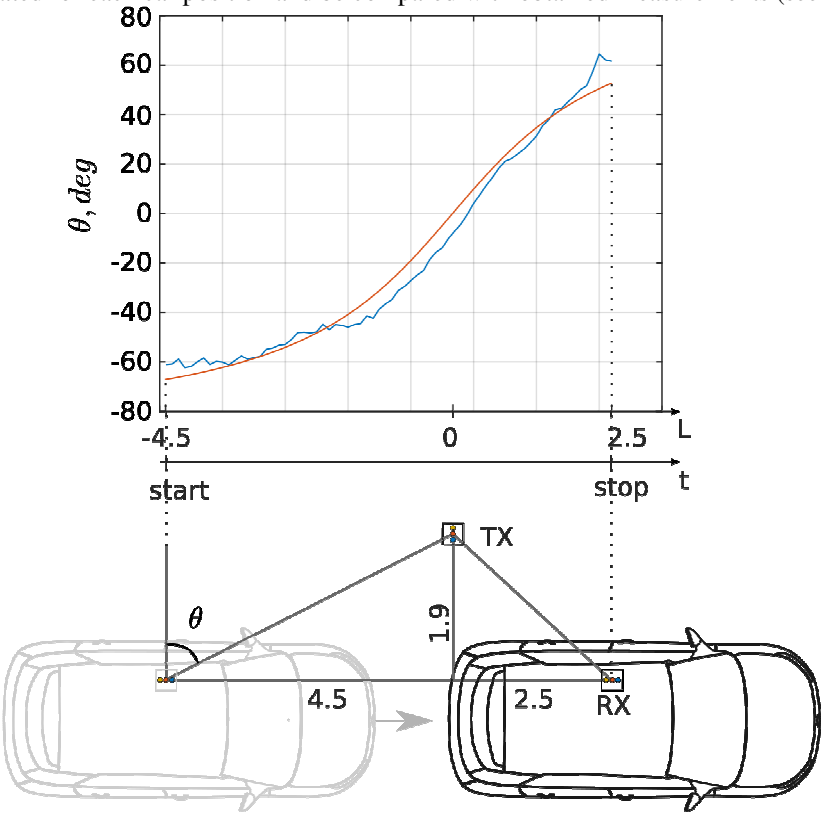

Figure 20 – True (red) and estimated (blue) angles during the car experiments

The car experiments show that the angle estimation accuracy has degraded (see the red graph on the Figure 18). The car influence is significant. The CST model should be corrected for the car body considering. Otherwise, the angle estimation accuracy would be about 10 degrees.

Angles estimation errors under multipath condition

We repeated the tripod experiments under poor propagation conditions. The mockups were located in a covered public parking (see Figure 21). It is heavy environment for radio signals. There is a low ceiling, close columns and other cars. As a result, observations histograms have a few peaks and are wide enough (see Figure 17, b).

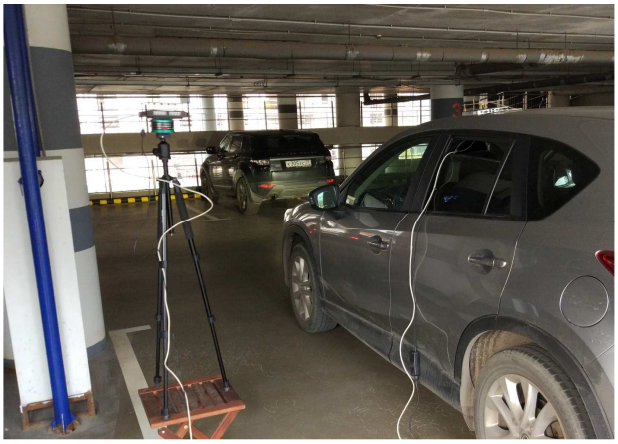

Figure 21 - The experiment in the bad propagation condition (parking)

In comparison with the open area results, the angle estimation accuracy is a little worse by RMSE and significant worse by peak value (see the gold graph on the Figure 18).

Let's try to increase the signal bandwidth from 10 MHz to 20 MHz. We can utilize all subcarriers from received log files for this purpose. Angle estimations errors for this case are presented on the Figure 22.

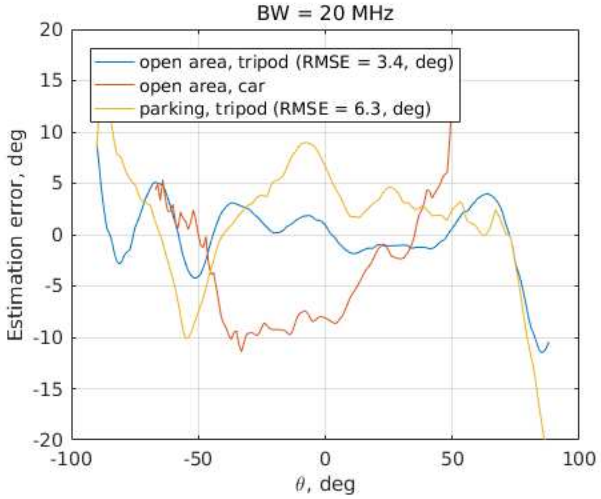

Figure 22 – Angle estimation errors for the 20 MHz signal bandwidth (CST RPs are still used)

The wider bandwidth didn't improve the open area results, but peak error for parking experiments decreased by 5 degrees. The twice bandwidth reduces the multipath error approximately twice and doesn't effect to the mutual influence. Consequently, the multipath error can be roughly estimated as 10 degrees of peak value in the parking experiment.

CONCLUSION

DSRC signals can be used for vehicle-to-vehicle angular measurements. The DSRC signals are widespread, have good bandwidth and enough power. The safety messages are transmitted by means of these signals, so the signals have high priority and stable period. The receiver of the signals can measure both own orientation to the line-of-sight and the transmitter one. As result, the cooperative network gets two independent measurements of each angle and can check these values. The angle estimation signal processing algorithm is presented. The algorithm can be used with different types of antenna systems. It utilizes steering vectors which are calculated from antenna radiation patterns. It is shown, that the main error sources are: a) the radiation patterns distortion due to mutual influence of antenna elements and vehicles; b) the multipath signal propagation. In the study we focused on a uniform linear array of three vertical vibrators as the antenna system. The mutual influence of the antenna elements was estimated by means of an electromagnetic simulation. The simulation results were approved by field experiments. The simulation amendments allow to decrease angle-of-arrival estimation errors from about 10 to 2-3 degrees RMSE or 5 degrees of peak error. Due to these experiments it is shown that the presented algorithm can estimate angles-of-departure with the similar accuracy. If the antennas are mounted on the car body, it significantly effects on the radiation patterns. The unaccounted influence of the car body to the patterns contributes up to ten degrees to the angle estimation error. In the direct line-of-sight conditions multipath contribution in common error is about 10 degrees.

ACKNOWLEDGMENTS

This work was supported by the Ministry of Education and Science of the Russian Federation (project no. 8.9615.2017/BCh). The authors are grateful to Igor Tsarik (Amungo Navigation) for his assistance in the electromagnetic simulation and useful recommendations. The estimation algorithm synthesis approach is inspired by Vladimir N. Kharisov.

REFERENCES

(SAEJ2945/1) SAE J2945/1: "Surface Vehicle Standard: On-board Systems Requirements for V2V Safety Communications", 2015

(SAEJ2735) SAE J2735: "Dedicated Short Range Communication (DSRC) Message Set Dictionary", 2016

(ETSITS102637-2) ETSI TS 102 637-2: "Intelligent Transport Systems (ITS); Vehicular Communications; Basic Set of Applications; Part 2: Specification of Cooperative Awareness Basic Service", 2011

(ETSIES202663) ETSI ES 202 663: "Intelligent Transport Systems (ITS); European profile standard for the physical and medium access control layer of Intelligent Transport Systems operating in the 5 GHz frequency band", 2009

(IEEE1609.3) IEEE Std 1609.3-2016 "IEEE Standard for Wireless Access in Vehicular Environments (WAVE) — Network Services". 2016

(IEEE1609.4) IEEE Std. 1609.4-2016 "IEEE Standard for Wireless Access in Vehicular Environments (WAVE) -- Multi-Channel Operation", 2016

(IEEE802.11p) IEEE Std. 802.11p-2010 "IEEE Standard for Information Technology—Telecommunications and Information Exchange Between Systems—Local and Metropolitan Area Networks—Specific Requirements Part 11, Wireless LAN Medium Access Control (MAC) and Physical Layer (PHY)", 2010.

(Chen2012) H.C. Chen et al., "Determining RF angle of arrival using COTS antenna arrays: A field evaluation", MilCom, 2012

(Paun2015) Mirel Paun, Razvan Tamas, Ion Marghescu, "Angle-of-Arrival Estimation in Multipath Environments Using Sliding Antenna Arrays", Progress In Electromagnetics Research Letters, Vol. 54, 101–105, 2015

(Tichonov1991) V. I. Tikhonov, V. N. Kharisov, "Statistical Analysis and Synthesis of Radio Engineering Devices and Systems", Radio i Svyaz', Moscow, 1991

(Cheong2015) Joon Wayn Cheong, Eamonn Glennon, Andrew Dempster, Damien Serant, Thibaud Calmettes, "Modelling and Mitigating Multipath and NLOS for Cooperative Positioning in Urban Canyons", 2015

(AcostaMarum2007) G. Acosta-Marum, M. A. Ingram, "Six Time- and Frequency- Selective Empirical Channel Models for Vehicular Wireless LANs", IEEE 66th Vehicular Technology Conference, pp.2134-2138, 2007

(Yin2006) Jijun Yin, Gavin Holland, Tamer Elbatt, Fan Bai, Hariharan Krishnan, "DSRC channel fading analysis from empirical measurement," in Proceedings of the 1st IEEE International Workshop on Vehicle Communications and Applications (Vehiclecomm), Beijing, China, October 2006.

(Islam2013) T. Islam, B. Boltjes, Y. Hu, E. Onur, J.F.C.M de Jongh, "Realistic Simulation of IEEE 802.11p Channel in Mobile Vehicle to Vehicle Communication," 13th International Conference on Microwave Techniques (COMITE), Pardubice, Czech Republic, April 17-18, 2013

(Kukolev2015) P. Kukolev, A. Chandra, T. Mikulasek, and A. Prokes, "Out of vehicle channel sounding in 5.8 GHz band," Proc. IEEE RNDM, pp. 341–344, Oct. 2015

(Keysight2016) Keysight Technologies, "Solutions for 802.11p Wireless Access in Vehicular Environments (WAVE) Measurements", Application Note 5992-1353EN, USA, October 31, 2016

(Kotaru2015) M. Kotaru, K. Joshi, D. Bharadia, S. Katti, "Spotfi: Decimeter level localization using wifi"`, ACM SIGCOMM Computer Communication Review, volume 45, 269-282, 2015

(Halperin2011) D. Halperin, W. Hu, A. Sheth, and D. Wetherall, "Tool Release: Gathering 802.11n Traces with Channel State Information." ACM SIGCOMM CCR, 41(1):53, Jan. 2011

(Halperin2009) D. Halperin, "Two Antennas are Better than One: A Measurement Study of 802.11n, dhalperi.github.io/linux-80211n-csitool, University of Washington, 2009.

(Korogodin2012) Korogodin I.V., Bukreev A.M., "Compensation for the Difference between Phase Shifts in the RF Blocks of Goniometric GLONASS Receivers", Radiotechnika, No 6, pp. 140-147, 2012

(Schüssel 2016) Martin Schüssel. “Angle of Arrival Estimation using WiFi and Smartphones”, Intl. Conf. Indoor Positioning and Indoor Navigation, Spain, 2016.

(Tzur2015) Asaf Tzur, Ofer Amrani, and Avishai Wool, “Direction Finding of rogue Wi-Fi access points using an off-the-shelf MIMO–OFDM receiver”, Physical Communication, 2015.

(Wong2008) C. Wong, R. Klukas, G.G. Messier, “Using WLAN infrastructure for angle-of-arrival indoor user location”, VTC Fall, IEEE, pp. 1–5, 2008,

(CSITool) http://dhalperi.github.io/linux-80211n-csitool